Physicochem. Probl. Miner. Process., 61(1), 2025, 202595

http://www.journalssystem.com/ppmp

Physicochemical Problems of Mineral Processing

ISSN 1643-1049

Effect of flocculation behavior on the flotation of synthetic apatite-dolomite mixtures based on FBRM and PVM

Guixu He [1], Aoao Chen [1], Lina Zhao [1], Qin Zhang [2], Wubin Li [2], Jun Xie [2,3], Jieliang Wang[2,4]

[1] Mining College, Guizhou University, Guiyang 550025, China

[2] Guizhou Academy of Sciences, Guiyang 550001, China

[3] Department of Materials Science and Engineering, Anhui University of Science and Technology, Huainan 232001, China

[4] School of Mining and Coal Engineering, Inner Mongolia University of Science and Technology, Baotou 014010, China

Corresponding author: zq6736@163.com (Qin Zhang)

Abstract: This study investigates the influence of various factors on shear flocculation in the apatite-dolomite mixed ore flotation system. The Box-Behnken response surface methodology is employed to evaluate the interactions of these factors on flocculation behavior. Additionally, the Focused Beam Reflectance Measurement (FBRM) and Particle Vision Measurement (PVM) techniques are applied to investigate the mechanisms by which these factors affect shear flocculation. The results show that sodium oleate (NaOL) concentration, pH, and shear rate significantly influence the size of the flocculated particles. Notably, the interaction effect between NaOL concentration and pH is particularly pronounced. FBRM and PVM analysis reveals that pH and NaOL concentration play dominant roles in controlling particle flocculation, while H_3PO_4 has a relatively minor impact on agglomerate morphology and size. At low shear rates, the flocs are larger and more uniformly distributed, resulting in a more stable process. In contrast, although high shear rates enhance initial flocculation efficiency, they reduce floc size. Furthermore, the modified Smoluchowski model is applied to evaluate the impact of different factors on flocculation kinetics. The findings suggest that the effects of these factors vary across different stages of flocculation. The combined influence of NaOL concentration, pH, and shear rate is crucial in determining the stability of the flocs, with these three factors being key determinants of floc morphology and stability.

Keywords: FBRM, apatite, dolomite, response surface methodology, flocculation kinetics, flotation

1. Introduction

Phosphorus is an essential element in various fields, including agriculture, chemistry, medicine, and new energy materials (Zhang et al., 2024). Phosphorite is a primary source of phosphorus, with apatite as its main valuable component, while the principal gangue minerals include dolomite, calcite, and quartz (Xie, 2024). Phosphate ores can be classified into siliceous, calcareous-magnesium, and silico-calcareous types based on the gangue mineral composition (Shi, 2017). Calcareous-magnesium phosphate ores, which have a higher dolomite content, significantly hinder the effective separation of apatite and dolomite during flotation. Since apatite and dolomite share similar surface properties, their flotation behavior is also comparable. The collector interacts with the surface sites of both minerals similarly (Zhang et al., 2023), resulting in only minor flotation differences. Additionally, fine slimes often form during grinding, further complicating the flotation process and worsening the separation efficiency (Ruan et al., 2018). Consequently, conventional flotation methods struggle to achieve effective separation. To address these challenges, researchers are exploring new technologies to improve flotation efficiency, including flotation columns, hydrophobic aggregation flotation, microbubble flotation, ultrasound-assisted flotation, and the development of novel, high-efficiency reagents (Ruan et al., 2019). Among these, hydrophobic aggregation flotation has gained significant attention as an effective approach to enhance fine particle flotation (Niu et al., 2024). It has been widely studied for fine

DOI: 10.37190/ppmp/202595

mineral separations in ores such as molybdenite, tungsten, bauxite, and clay minerals (Yang, 2020). However, research on hydrophobic aggregation flotation for phosphate ores remains limited.

Shear flocculation is an effective method for promoting hydrophobic aggregation, as it utilizes fluid shear forces to provide sufficient energy to overcome energy barriers (Li et al., 2021; Pascoe et al., 1997), while also increasing the collision frequency between particles (Luo et al., 2021). This leads to the formation of larger aggregates from fine particles, which have enough strength to withstand the turbulent forces in the slurry (Cai et al., 2019), resulting in the stable formation of hydrophobic aggregates (Yang et al., 2020). Achieving the proper balance between shear intensity and reagent selection is critical for both the formation and stability of these aggregates (Yang et al., 2018).

In previous studies, offline techniques such as laser diffraction and optical microscopy have been primarily used to characterize the particle size and morphology of aggregates. However, offline measurements are limited in frequency, which can result in incomplete descriptions of particle size distributions. Additionally, sample extraction and handling can disturb the aggregates, potentially affecting the accuracy of the measurements (Ye et al., 2020).

In contrast, online techniques such as Focused Beam Reflectance Measurement (FBRM) and Particle Vision Measurement (PVM) provide more reliable real-time characterization of the aggregation process during shear flocculation of fine apatite and dolomite particles. FBRM enables continuous monitoring of particle size and distribution changes within the slurry, offering immediate feedback on the effects of reagents and shear forces on aggregation, while also allowing for the quantification of flocculation efficiency (Grabsch et al., 2020). Meanwhile, PVM provides visual insights into particle morphology and the aggregation structure in the slurry. The combination of these techniques allows for both quantitative and qualitative analysis of the flocculation process. This integrated monitoring approach provides valuable process data for the flotation and separation of fine apatite and dolomite particles.

FBRM and PVM enable real-time monitoring of particle growth, breakage rates, and changes in agglomeration morphology, offering deeper insights into the flocculation dynamics during the flotation process (Chimonyo et al., 2022). Li et al. (Li et al., 2017) investigated the flocculation trends of fine and coarse hematite particles at different mixing ratios using FBRM, providing insights into how these trends affect flotation performance. Wang et al. (Wang et al., 2021) used the Extended Derjaguin-Landau-Verwey-Overbeek Theory (EDVLO) to explain the interactions between fine and coarse particles in coal slime flotation and observed with FBRM and PVM that the improved flotation performance of fine coal was due to the aggregation of fine particles with coarse coal particles. Duan (Duan, 2022) measured particle size changes during the flocculation of fine coal slurries using FBRM, finding that floc size initially increased and then decreased with increasing flocculant dosage, and increased first before rapidly decreasing as shear rates increased. These studies collectively demonstrate that the combination of FBRM and PVM offers a clear understanding of the aggregation behavior of fine particles, which can also be applied to study the aggregation behavior of fine phosphate ores.

Although considerable research has been conducted on the flocculation behavior of minerals during phosphate flotation, several studies have made significant contributions. For instance, Huang et al. (Huang et al., 2023) investigated the interactions between fine and coarse dolomite particles and their impact on flotation. Using cryogenic scanning electron microscopy, they observed the agglomeration effect of fine dolomite on coarse dolomite and coarse apatite particles. However, the process is relatively complex and typically suited for static analysis. Zhao et al. (Zhao et al., 2024) used laser diffraction and rheometry to analyze the particle size and rheological properties of apatite after shear flocculation. Their results showed that as apatite particles aggregated, a network structure formed in the slurry, impeding fluid flow and increasing slurry viscosity. Yang et al. (Yang et al., 2018) employed an infrared turbidity meter to evaluate the aggregation of apatite particles in suspension and used digital image analysis to observe the aggregates under a microscope and calculate their fractal dimension. They found that, at appropriate concentrations of sodium oleate and stirring speeds, the aggregation of apatite particles was more effective, leading to more uniform aggregates. While these techniques provide valuable data on particle size and rheological properties, they are limited in their ability to accurately describe particle morphology and often require complex sample preparation and image analysis. Therefore, utilizing FBRM and PVM to study the aggregation behavior of fine phosphate particles during flotation offers distinct advantages, as these methods provide clearer insights, especially under dynamic process conditions.

In this study, a Box-Behnken design (BBD) response surface methodology was employed to investigate the flocculation behavior and flotation performance of apatite and dolomite in artificially mixed fine phosphate ores under varying conditions. FBRM, PVM, and the modified Smoluchowski model were used to analyze the shear flocculation process of the mixed ores and their correlation with flotation recovery. The results highlighted the impact of four key factors on shear flocculation and their relationship with flotation recovery, providing a foundation for improving the flotation separation of fine phosphate ores.

2. Materials and methods

2.1. Materials

The phosphate ores used in this study were sourced from Guizhou, China. Apatite and dolomite were handpicked, crushed to below 2 mm, and then ground in a 1 dm^3 alumina ball mill jar (XBM) using alumina ceramic balls with a 40% filling rate. A 100 g of each mineral was ground to a slurry concentration of 30% to 35% with apatite and dolomite ground for 6 min and 2 min. After the grinding, the slurry was screened at 75 μm, and the oversized fraction was returned to the alumina ball mill jar for regrinding until all material passed through the sieve. All samples were filtered to remove excess slurry and then dried at 50°C. The particle size distributions of the samples are shown in **Błąd! Nie można odnaleźć źródła odwołania.**.

The XRD patterns of the samples are shown in Fig. 2, with detailed XRF analysis data provided in Table 1 (He et al., 2023). XRD analysis demonstrates that both purified mineral concentrates maintain low impurity levels. Quantitative chemical analysis reveals that the apatite concentrate contains 38.0% P_2O_5 and 3.5% F, achieving 93% theoretical purity with associated dolomite and siliceous minerals. While the dolomite concentrate contains 29.0% CaO and 20.4% MgO, reaching 94% purity with trace apatite and siliceous minerals. These results confirm the high purity of the mineral concentrates, meeting the experimental requirements for subsequent investigations.

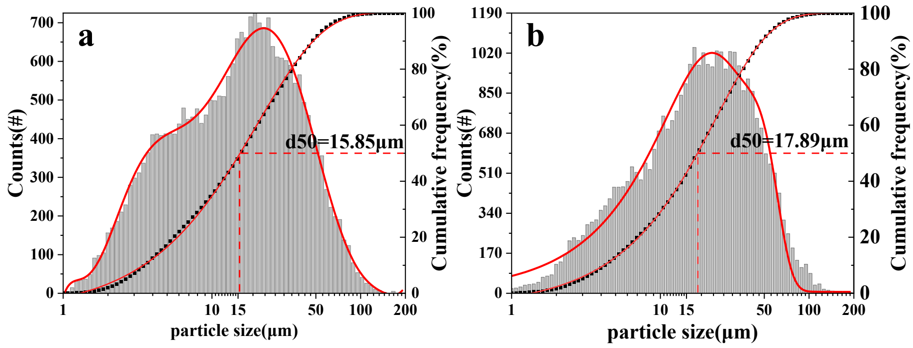

Fig. 1. Particle size distribution of the sample: (a) Apatite, (b) Dolomite

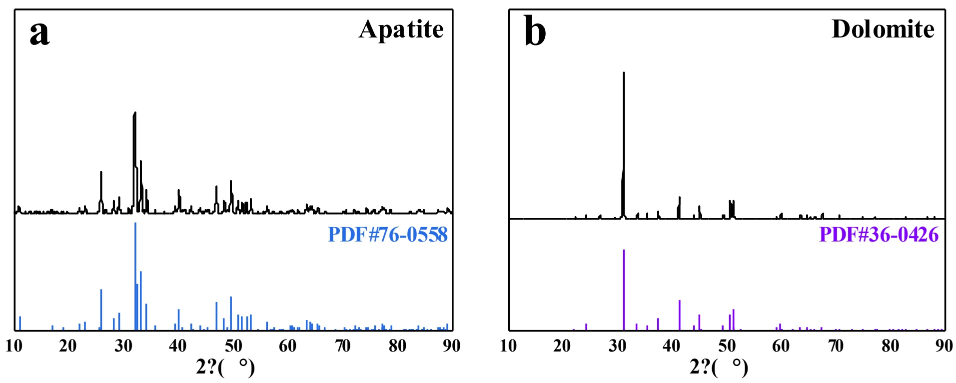

Fig. 2. XRD patterns of apatite and dolomite

Table 1. XRF analysis of apatite and dolomite

Sample	Content/ %				
	P_2O_5	CaO	MgO	SiO_2	F
Apatite	38.00	53.00	0.15	1.39	3.50
Dolomite	0.27	29.00	20.40	4.98	<0.10

The collector sodium oleate (NaOL) was obtained from Macklin, the depressant phosphoric acid (H_3PO_4) from Chuandong Chemicals, and the pH adjusters hydrochloric acid (HCl) and sodium hydroxide (NaOH) from Chuandong Chemicals and Kermel, respectively.

2.2. Methods

2.2.1. Response surface experimental design

The Box-Behnken experimental design is a method based on response surface methodology. By constructing a second-order mathematical model, it analyzes the relationship between response variables and experimental factors, effectively capturing the nonlinear effects of factors on response values and elucidating the interactions between factors during the experimental process (Wang et al., 2024; Zhang et al., 2024). The general form of its second-order model is:

$$Y=\beta_0+\sum\beta_i X_i+\sum\beta_{ii} X_i^2+\sum\beta_{ij} X_i X_j+\varepsilon \tag{1}$$

In this model, β_0 is the constant term, β_i represents the coefficient of the linear terms, β_{ii} is the coefficient of the quadratic terms,β_{ij} is the coefficient of the interaction terms, and ε represents the error term. X_i and X_j are the levels of the factors. The interaction term $\beta_{ij}X_iX_j$ reflects the synergistic or inhibitory effects between two factors.

Based on the principles of the Box-Behnken experimental design, a series of experiments were conducted to investigate the factors affecting micro-flotation, including collector concentration, depressant concentration, pH, and shear rate. A 4-factor, 3-level response surface experiment was designed with mean particle size (Y) as the response variable.

2.2.2. FBRM and PVM experiments

FBRM technology enables real-time monitoring of changes in the chord length of particles and aggregates in the slurry. The principle behind this technique involves a sapphire probe emitting a focused laser beam that scans the particles or aggregates flowing through its detection area. When the laser intersects a particle or aggregate, part of the light is reflected to the probe, transmitted via optical fibers, and detected by a photodiode, as shown in Fig. 3.

The duration of the backscattered light is proportional to the particle size. Since the laser scanning speed is set at 2 m/s, the time it takes for the laser to scan a particle can be directly related to its chord length (Boxall et al., 2010). The chord length calculation formula is given in Eq. (2):

$$S=v_b\times(t_2-t_1) \tag{2}$$

In Eq. (2), S represents the particle chord length (μm), v_b is the scanning speed (μm/s), t_1 and t_2 are the times (s) when the laser scans the start and end points of the particle chord length, respectively. The probe can detect the size distribution of mineral particles and aggregates ranging from 0.5 μm to 2000 μm during the experiment (Li et al., 2020).

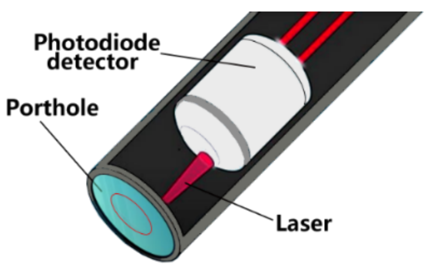

Fig. 3. Sapphire probe of FBRM (Lasentec, 2001)

PVM is an advanced online imaging tool primarily used for real-time monitoring of particle dynamics in the liquid phase. It captures changes in particle size, shape, and aggregation state through microscopic images, allowing direct observation of the formation, breakage, and time-dependent trends of particle aggregation during flotation.

In this study, both FBRM and PVM tests were conducted using the EasyMax 402 advanced synthesis reactor. The ParticleTrack G400 and ParticleView V19 (both Mettler Toledo, USA) were employed for FBRM and PVM measurements, respectively. Samples were introduced into the reactor according to the micro-flotation conditioning process described in Section 2.2.3. Data collection began immediately after the sample was added, and after the introduction of NaOL, measurements were taken every 2 sec for 180 sec, monitoring changes in particle count and size.

2.2.3. Micro flotation experiments

To simulate the slurry flow conditions in the FBRM test, a custom-built flotation apparatus was used for the micro-flotation experiments, as shown in Fig. 4. For each trial, 5 g of a prepared mineral sample (apatite 3: dolomite 1) was weighed and used in the artificial mixed flotation test. The flotation procedure is as follows: the sample is first conditioned for 1 min, followed by the addition of the depressant, pH adjustment, and then the addition of the collector. The pH adjuster and flotation reagents were allowed to react for 1 min and 3 min, respectively. The recovery rate of apatite in the artificially mixed ore was calculated using Eq. (3):

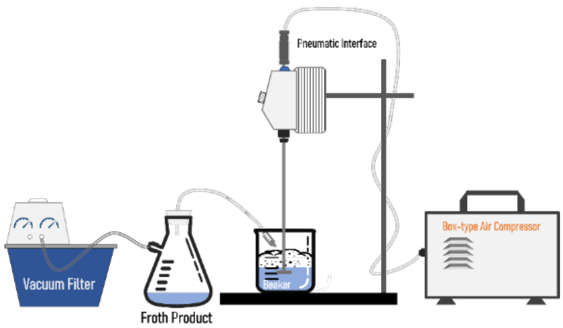

Fig. 4. Simplified diagram of equipment

$$R=\frac{c_s}{c_f+c_s}\times 100\% \tag{3}$$

In Eq. (3), R represents the recovery rate of the apatite, while c_f and c_s denote the mass of the floated product and the mass of the sink product, respectively.

3. Results and discussion

3.1. Response surface experiment

3.1.1. Development and analysis of the box-Behnken regression model

Response surface methodology (RSM) is used to model data and identify the most influential independent variables among multiple factors. Interaction terms also provide insights into the relationships between these variables (Hao et al., 2019). Using the Box-Behnken experimental design, a 4-factor, 3-level design was applied to study the effects of collector concentration (A), depressant concentration (B), pH (C), and shear rate (D). A total of 27 experimental runs were conducted, including 24 factorial runs and 3 center point replicates, as shown in Table 2.

Based on the results in Table 2, multivariate regression analysis was performed on Y and each factor using Design Expert software, yielding the following quadratic regression equation (Eq. 4):

$$Y=33.96+7.57A+2.49B-9.61C-8.70D-1.77AB-1.92AC-2.99AD-3.20BC-2.54BD+3.56CD-9.09A^2+0.3248B^2-5.66C^2+6.50D^2 \tag{4}$$

In Eq. (4), Y represents the mean particle size, and A, B, C, and D denote the collector concentration, depressant concentration, pH, and shear rate, respectively. The experimental results indicate that the coefficient of determination (R^2) reaches 0.9480, suggesting a good fit for the model. Therefore, the regression equation can be used to analyze the experimental results, as shown in Table 3.

As shown in Table 3, the P-value of the second-order regression model is less than 0.0001, indicating a highly significant result. The coefficient of determination (R^2) is 0.9480, meaning that the model explains 94% of the variation in the response, with good consistency between the predicted and observed values. The adjusted R^2 (R^2_{Adj}) is 0.8875, suggesting that 88.75% of the variability in the experimental outcomes can be attributed to the experimental factors. The predicted R^2 (R^2_{Pre}) is 0.7060, and the difference between R^2_{Adj} and R^2_{Pre} is 0.1815 (less than 2), indicating that the model is not overfitted and has satisfactory predictive capability. The model's Adeq Precision, with a value of 16.2899 (greater than 4), confirms the adequacy of the model for navigating the design space. The lack of fit (0.1338 > 0.05) is not significant, indicating that the model fits the experimental data well without any significant lack of fit.

The impact of the independent variables on the dependent variable in the response surface analysis can be assessed through significance testing in the analysis of variance (ANOVA). As shown in Table 3, factors A, C, and D have a highly significant effect on Y ($P < 0.01$), while factor B does not significantly affect Y ($P > 0.05$). In the model, the quadratic terms A^2 and D^2 have a highly significant effect on Y, C^2 has a significant effect, and B^2 is not significant.

As indicated by the previous analysis, NaOL concentration, pH, and shear rate have a significant individual effect on the flocculation of the mixed ore during flotation. However, in slurry systems, particle flocculation is often influenced by the combined effects of multiple factors. Therefore, analyzing the interacti on terms of these factors in the response surface model is crucial.

Table. 2. Response surface methodology and experimental results

Std.	**Collector Concentration (mol/dm^3) A**	**Depressant Concentration (mol/dm^3) B**	**pH C**	**Shear Rate (S^{-1}) D**	**Mean Particle Size (μm) Y**
1	5.50×10^{-4}	1.00×10^{-4}	3	55.0	28.26
2	1.00×10^{-4}	5.05×10^{-3}	3	55.0	22.14
3	5.50×10^{-4}	1.00×10^{-4}	7	36.6	45.94
4	1.00×10^{-4}	5.05×10^{-3}	7	73.4	15.91
5	1.00×10^{-3}	5.05×10^{-3}	7	73.4	27.91
6	1.00×10^{-3}	5.05×10^{-3}	3	55.0	34.18
7	5.50×10^{-4}	5.05×10^{-3}	7	55.0	36.02
8	1.00×10^{-4}	5.05×10^{-3}	11	55.0	8.02
9	5.50×10^{-4}	5.05×10^{-3}	3	36.6	60.29
10	1.00×10^{-3}	1.00×10^{-2}	7	55.0	20.79
11	5.50×10^{-4}	1.00×10^{-2}	3	55.0	41.29
12	5.50×10^{-4}	1.00×10^{-4}	7	73.4	29.48
13	1.00×10^{-4}	5.05×10^{-3}	7	36.6	24.18
14	5.50×10^{-4}	1.00×10^{-4}	11	55.0	17.69
15	1.00×10^{-3}	1.00×10^{-4}	7	55.0	37.84
16	1.00×10^{-4}	1.00×10^{-2}	7	55.0	20.79
17	5.50×10^{-4}	5.05×10^{-3}	3	73.4	36.78
18	1.00×10^{-3}	5.05×10^{-3}	7	36.6	48.13
19	5.50×10^{-4}	5.05×10^{-3}	11	73.4	21.13
20	5.50×10^{-4}	5.05×10^{-3}	7	55.0	33.02
21	5.50×10^{-4}	1.00×10^{-2}	11	55.0	17.93
22	1.00×10^{-4}	1.00×10^{-4}	7	55.0	15.06
23	5.50×10^{-4}	5.05×10^{-3}	7	55.0	32.83
24	5.50×10^{-4}	1.00×10^{-2}	7	36.6	57.12
25	1.00×10^{-3}	5.05×10^{-3}	11	55.0	12.40
26	5.50×10^{-4}	5.05×10^{-3}	11	36.6	30.41
27	5.50×10^{-4}	1.00×10^{-2}	7	73.4	30.48

Table. 3. Model ANOVA and significant test table

Source	Sum of Squares	df	Mean Square	F-value	p-value
Model	4131.72	14	295.12	15.65	< 0.0001**
A-Collectors	688.24	1	688.24	36.49	< 0.0001**
B-Depressant	74.15	1	74.15	3.93	0.0707
C-pH	1109.17	1	1109.17	58.81	< 0.0001**
D-Gs	907.74	1	907.74	48.13	< 0.0001**
AB	12.51	1	12.51	0.66	0.4312
AC	14.69	1	14.69	0.78	0.3949
AD	35.71	1	35.7205443	1.89	0.1939
BC	40.92	1	40.92	2.17	0.1665
BD	25.89	1	25.89	1.37	0.2641
CD	50.61	1	50.61	2.68	0.1273
A^2	440.70	1	440.70	23.37	0.0004
B^2	0.56	1	0.56	0.03	0.8657
C^2	170.59	1	170.59	9.04	0.0109
D^2	225.30	1	225.30	11.95	0.0047
Residual	226.32	12	18.86		
Lack of Fit	219.90	10	21.99	6.86	0.1338
Pure error	6.41	2	3.20		
Cor Total	4358.04	26	Adeq Precision= 16.2899		
R^2=0.9480			R^2 *Adj*= 0.8875		R^2 *Pre*= 0.7060

3.1.2. Two-factor interaction response surface analysis

The 3D response surface plots demonstrate the significance of two-factor interaction effects. These interaction terms illustrate how changes in one factor's level can influence the effect of another factor on the response variable. By analyzing the fitted data, 3D response surface plots were generated to depict the interactions between collector concentration, depressant concentration, pH, and shear rate, as shown in Fig. 5.

In 3D response surface plots, contour lines, surface steepness, and color gradients offer insights into the interaction effects and their impact on the response variable (Wang et al., 2024). More elliptical contour lines indicate stronger interactions between factors, while those closer to circular shapes suggest weaker interactions (Li et al., 2015).

As shown in Fig. 5c, the particle size initially increases and then decreases with rising NaOL concentration and reducing shear rate. A prominent peak occurs when the collector concentration is between 5×10^{-4} and 1×10^{-4} mol/dm^3 and the pH is between 5 and 6. In Fig. 5, the surface displays the steepest gradient, and the contour lines are both closely spaced and elliptical, indicating a significant interaction between NaOL concentration and pH. Building upon previous research on fine particle flotation, at high pH, NaOL predominantly exists as $RCOO^-$, which increases its solubility in solution and weakens its adsorption capacity on the mineral surface. The ΔG for the reaction between oleate ions and Ca^{2+} becomes smaller (Zhang et al., 2011), making the adsorption process less favorable. Additionally, at higher pH, NaOL is less effective at forming mineralized froth, and the hydrophobic forces between particles are weakened, which prevents agglomeration (Zhao et al., 2022) and leads to a significant decrease in recovery (Wang, 2020). In Fig. 5a, 5d, 5e and 5f, the surfaces are relatively flat, and the contour lines are sparse, indicating that the interaction between the other factors is not significant.

The analysis of variance (ANOVA) and two-factor interaction analysis reveals that the solution chemistry of NaOL and pH are critical factors influencing particle behavior. Within an optimal pH range, NaOL significantly enhances the hydrophobicity of the particle surface by undergoing molecular transformations, such as the conversion of NaOL to OL^-, thus facilitating particle aggregation. However, when the pH exceeds this optimal range, the molecular activity of NaOL is reduced, leading to a substantial decrease in its adsorption capacity and, consequently, its ability to promote aggregation. Furthermore, the interaction between NaOL concentration and shear rate plays a pivotal role in the aggregation process. Moderate shear rates increase particle collision frequency and adsorption efficiency, fostering the formation of stable agglomerates. In contrast, excessively high shear rates disrupt agglomerates through mechanical forces, resulting in particle re-dispersion and a loss of aggregation stability.

The observed interaction effects indicate that the interplay of various factors not only controls the changes in particle size but also significantly affects the fundamental mechanisms of inter-particle interactions. However, the exact dynamics of particle aggregation and dispersion—particularly the formation, stability, and shear-induced breakage of flocs during the flotation process—are still not fully understood. Therefore, the following sections will provide a detailed analysis of how these factors influence flocculation behavior and their overall impact on flotation efficiency.

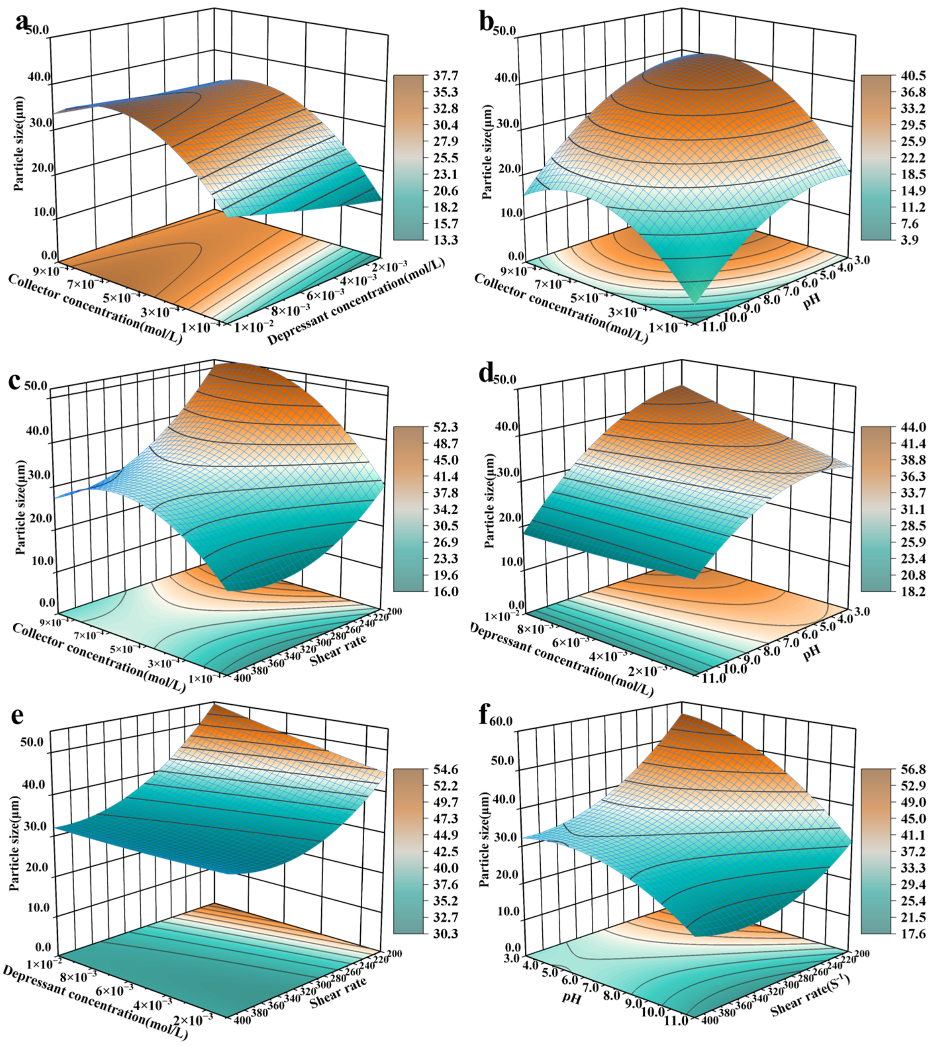

Fig. 5. 3D plot of the interaction effects among various factors: (a) AB: Collector and depressant, (b) AC: Collector and pH, (c) AD: Collector and shear stress, (d) BC: Depressant and pH, (e) BD Depressant and shear stress, (f) CD: pH and shear stress

3.2. Factors influencing particle agglomeration behavior

The effectiveness of flocculation in particle agglomeration flotation is a key factor affecting the recovery of flotation products and their subsequent rise to the surface. To further examine the impact of the four factors on particle size distribution within the response surface framework, selected grid points from the experimental design were analyzed. A three-dimensional particle size distribution plot, illustrating the evolution of the entire particle size range over time, was generated based on FBRM results, as shown in Fig. 6.

Fig. 6 demonstrates 3D particle size distribution plots under varying conditions of NaOL concentration, H_3PO_4 concentration, pH, and shear rate. Specifically, Fig. 6a depicts the baseline factor levels, while Fig. 5b and Fig. 5f correspond to NaOL concentrations, Fig. 6c and Fig. 6g represent H_3PO_4 concentrations, and Fig. 6c, Fig. 6e, Fig. 6d and Fig. 6h illustrate the effects of different pH values and shear rates. The 3D particle size distribution plots in Fig. 6 reveal significant changes in particle size distribution across the varying levels of these factors. For instance, in the absence of NaOL, the sample predominantly consists of fine particles; however, with the addition of NaOL, a marked increase in the number of particles in the medium size range is observed, shifting the distribution from a single peak (normal distribution) to a bimodal distribution.

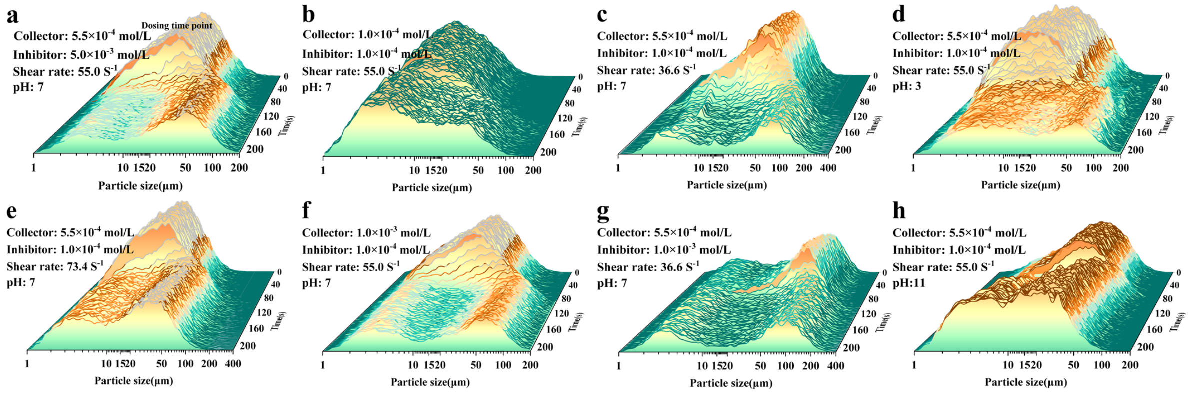

Fig. 6. 3D plot of particle size distribution over time

Analysis of Fig. 6a indicates that in the absence of NaOL, the particle distribution remains relatively dispersed with predominantly small particle sizes. This dispersion is due to weak van der Waals forces, which prevent particles from aggregating and keep them suspended in the solution (Wang et al., 2020). Upon the addition of NaOL, fine particles undergo rapid flocculation during the initial stage. As particle interactions peak, the floc structure stabilizes, exhibiting no significant decomposition or further aggregation. Consequently, flocculation behavior in this system can be divided into three distinct phases: (1) the initial rapid flocculation stage, where fine particles quickly combine to form larger flocs; (2) the intermediate slow growth phase, during which flocs gradually increase in size by attracting additional particles; and (3) the final stabilization phase, where agglomerates reach equilibrium under external forces, halting further growth and forming stable flocs (Gao et al., 2019; Wei et al., 2018).

To better elucidate the dynamic influence of collector concentration on particle agglomeration behavior, we utilized FBRM data to fit a function Np = f(t), where Np represents the particle count over time. By taking the first derivative of this function, the growth rate variations of particles across different size classes were determined. This approach facilitated a comprehensive analysis of how various factors affect particle size distribution and flocculation efficiency, providing deeper insights into the mechanisms governing particle aggregation dynamics.

3.2.1. Effect of collector dosage on particle size distribution

To examine the temporal evolution of particle counts across different size ranges, interpolation and curve fitting techniques were applied to the data, yielding the function Np = f(t). The first derivative of this function, f(t)', was analyzed to assess the direction (increase or decrease) and magnitude of changes in particle numbers within each size range. This analysis facilitated the construction of particle growth rate curves over flocculation time, as illustrated in Fig. 7.

Fig. 7a illustrates the particle size distribution curves under both low (1×10^{-4} mol/dm³) and high (1×10^{-3} mol/dm³) NaOL concentrations. At low concentrations, the values of $N_p'_{(10\text{-}45\ \mu m)}$ and $N_p'_{(45\text{-}75\ \mu m)}$ are negative, suggesting that medium-sized and larger particles undergo disaggregation. This is consistent with the observations of Jin (Jin, 2022), The underlying mechanism may be that at low concentrations, NaOL fails to form a complete hydrophobic layer on the particle surface (Gregory, 2013), leading to increased repulsive forces between flocculated particles. Consequently, these flocs become unstable and break apart under shear forces. In contrast, a comparison of Fig. 6b and Fig. 6f reveals that higher NaOL concentrations significantly enhance particle flocculation, as evidenced by the reduction of particles in the 1-20 μm range and the corresponding increase in larger particles in the 20-100 μm range. This indicates that elevated NaOL concentrations promote particle aggregation, consistent with previous studies (Li et al., 2021). Furthermore, the PVM images shown in Fig. 8 corroborate the FBRM results. Under low NaOL concentrations, particle flocculation is unstable, with some particles disaggregating and forming smaller flocs. At higher concentrations, the number of fine particles decreases while the number of coarse particles increases, aligning with the FBRM observations.

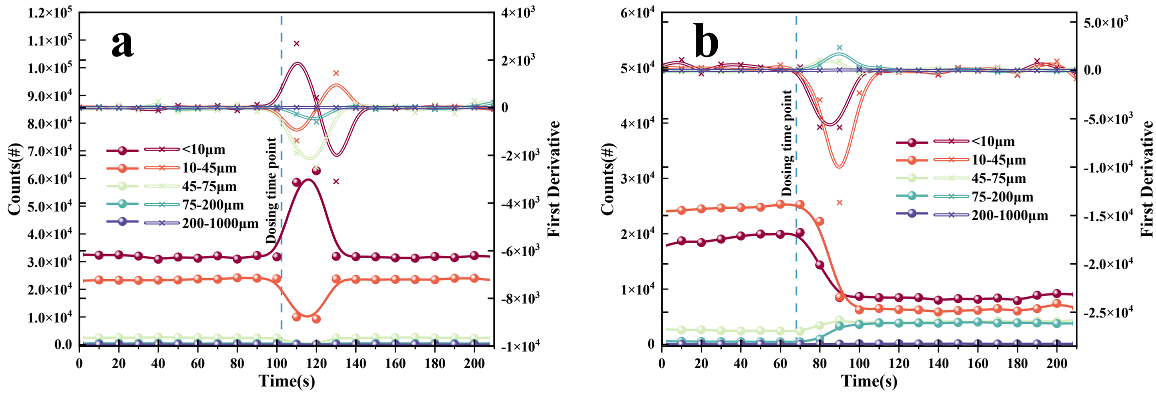

Fig. 7. Plot of particle size variation and first derivative: (a) Experiment 22 (NaOL concentration: 1×10^{-4} mol/dm^3), (b) Experiment 15 (NaOL concentration: 1×10^{-3} mol/dm^3)

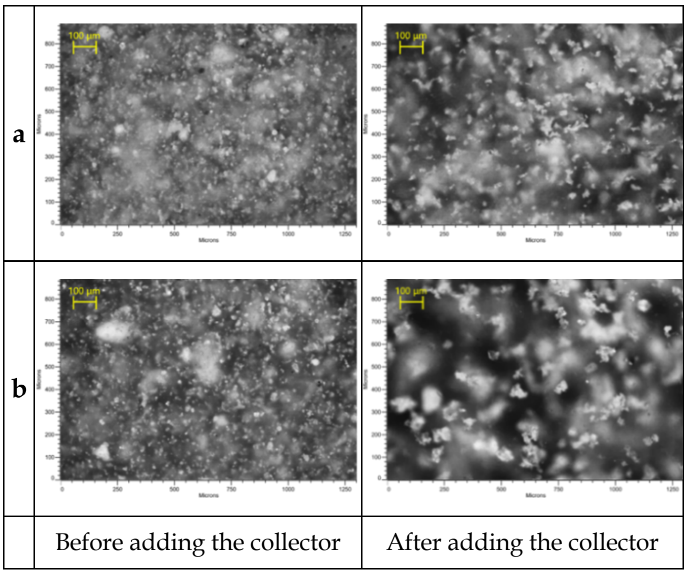

Fig. 8. PVM captured image of floc variation over time: (a) Experiment 22 (NaOL concentration: 1×10^{-4} mol/dm^3), (b) Experiment 15 (NaOL concentration: 1×10^{-3} mol/dm^3)

3.2.2. Effect of depressant dosage on particle size distribution

Fig. 9 illustrates the particle size distribution curves under both low (1×10^{-3} mol/dm^3) and high (1×10^{-2} mol/dm^3) H_3PO_4 concentrations. When comparing Fig. 9 with Fig. 6c and Fig. 6g it is evident that, regardless of H_3PO_4 concentration, the addition of NaOL results in a higher concentration of particle sizes in the 50–200 μm range. However, at higher concentrations of H_3PO_4, the distribution center shifts slightly to the right, leading to slightly larger particles. Following the addition of NaOL, Fig. 9a shows a drastic decrease in particles in the -10 μm and 10–45 μm ranges, with the particle count in the range of 45–75 μm first increasing before dropping and eventually stabilizing at zero. In contrast, particles in the 75–200 μm range gradually increase. The addition of NaOL significantly reduces the number of particles in the sub-200 μm size range and induces a slight increase in particles between 200–1000 μm, as shown in Fig 8b. This discrepancy can be attributed to the higher concentration of H_3PO_4 enhancing the negative charge of apatite (Huang et al., 2024), leading to a stronger influence of $H_2PO_4^-$ ions at the apatite-water interface (Ye, 2019), thereby increasing its hydrophilicity. However, the effect on the dolomite-water interface is relatively minor. This results in a reduction of apatite entrapment in dolomite aggregates (Wu et al., 2024), consequently limiting the occurrence of heterogeneous flocculation. As a result, flocculation is more likely to occur between particles with similar surface properties, leading to more stable aggregates with larger sizes. Further validation of these findings is provided by the micrographs in Fig. 10. In comparison to Fig. 10a, the aggregates in Fig. 10b are denser, more stable, and larger. Nevertheless, it is important to note that the impact of the depressant on particle aggregation is not as pronounced as the effect of NaOL.

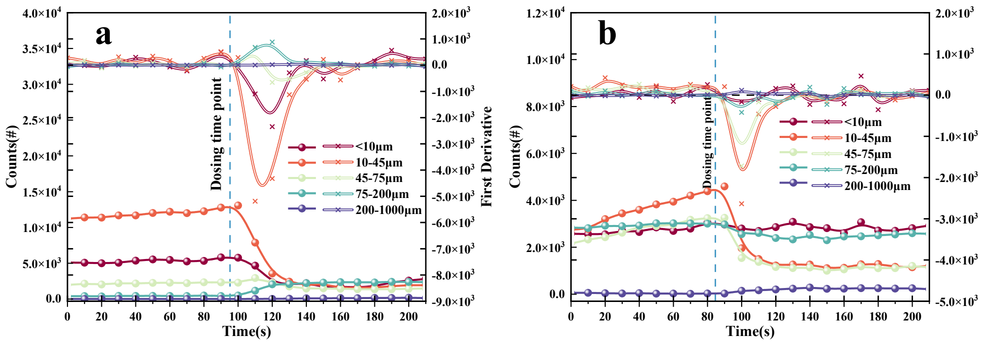

Fig. 9. Plot of particle size variation and first derivative: (a) Experiment 3 (Depressant concentration: 1×10-3 mol/dm3), (b) Experiment 24 (Depressant concentration: 1×10-2 mol/dm3)

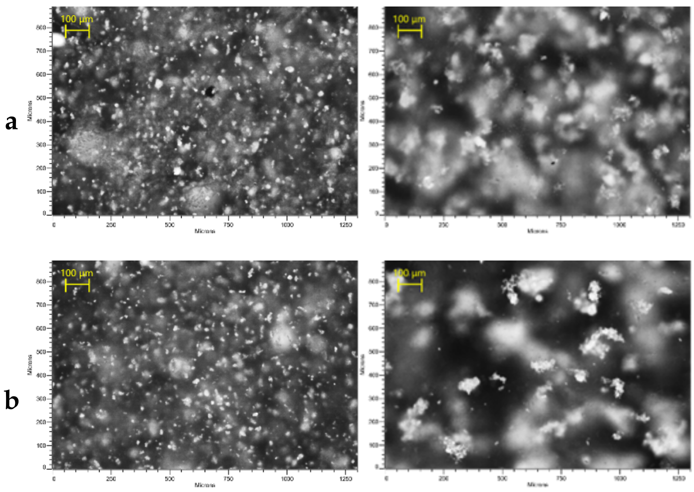

Before adding the collector After adding the collector

Fig. 10. PVM captured image of floc variation over time: (a) Experiment 3 (Depressant concentration: 1×10-3 mol/dm3), (b) Experiment 24 (Depressant concentration: 1×10-2 mol/dm3)

3.2.3. Effect of pH on particle size distribution

Fig. 11 presents the particle size distribution curves under both acidic and alkaline conditions at low and high pH levels. In Fig. 11, following the addition of NaOL under acidic conditions, the values for $N_{p}'_{(-10\ \mu m)}$ and $N_{p}'_{(10\text{-}45\ \mu m)}$ become negative, indicating a reduction in the number of fine particles. Meanwhile, the values for $N_{p}'_{(45\text{-}75\ \mu m)}$ and $N_{p}'_{(75\text{-}200\ \mu m)}$ gradually shift positively, suggesting the accumulation of mid-size and coarse particles. In alkaline conditions, similar negative trends are observed for $N_{p}'_{(-10\ \mu m)}$ and $N_{p}'_{(10\text{-}45\ \mu m)}$, but the magnitude of change is less pronounced, and the area enclosed by the curve around the x = 0 axis is smaller. Furthermore, a continuous increase in the values of $N_{p}'_{(-10\ \mu m)}$ and $N_{p}'_{(10\text{-}45\ \mu m)}$ is observed, indicating that flocculation under alkaline conditions is relatively weaker, resulting in less stable floc aggregates.

Fig. 12a and Fig. 12b display PVM images under acidic (pH 3) and alkaline (pH 11) conditions, respectively. As shown in Fig. 12a it can be observed that under acidic conditions, the aggregates formed by the particles are relatively small. This behavior can be attributed to two factors: first, the reaction of dolomite in acidic environments, and second, the increased hydrophilicity of apatite under acidic conditions, both of which diminish the aggregation tendency (Ye, 2019). Conversely, in Fig. 12b, under alkaline conditions, the addition of NaOL promotes the rapid formation of larger aggregates. However, these aggregates are not stable and eventually disintegrate into finer particles. This observation indicates that although flocculation is initially enhanced under alkaline conditions, the weak inter-particle interactions within the aggregates render them prone to breaking apart, preventing the formation of stable flocculates.

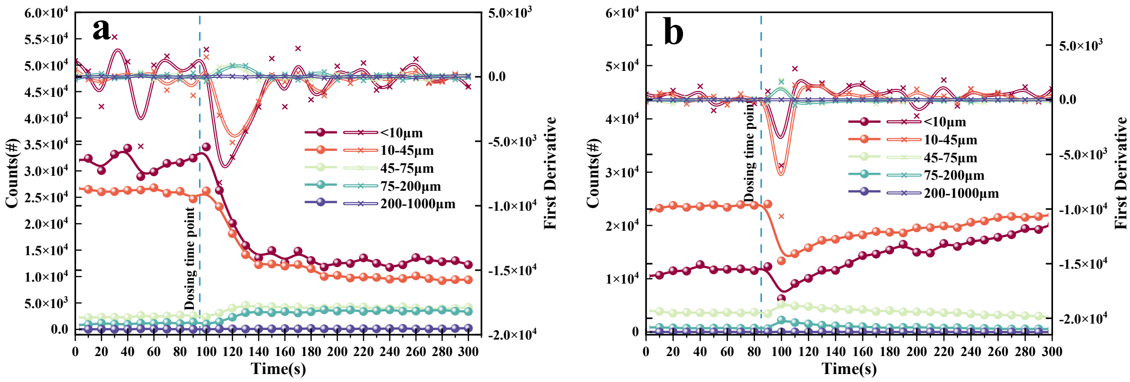

Fig. 1. Plot of particle size variation and first derivative: (a) Experiment 1 (pH=3), (b) Experiment 14 (pH=11)

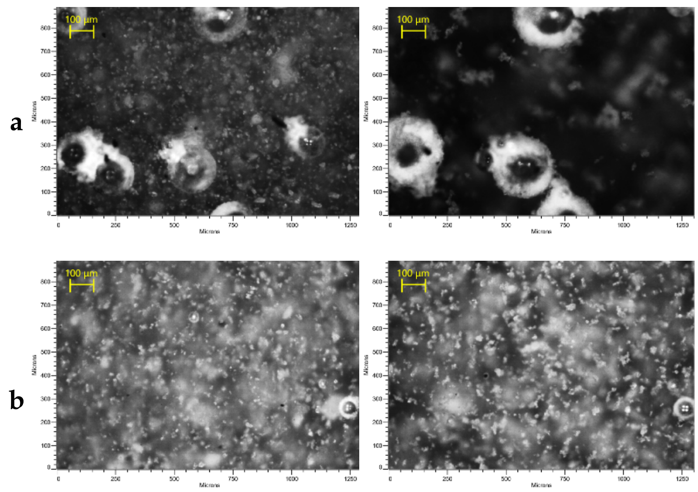

Before adding the collector After adding the collector

Fig. 12. PVM captured image of floc variation over time: (a) Experiment 1 (pH=3), (b) Experiment 14 (pH=11)

3.2.4. Effect of shear rate on particle size distribution

Fig. 13 illustrates the particle size distribution curves under both low (36.6 S^{-1}) and high (73.4 S^{-1}) shear rates. A detailed comparison between Fig. 6c, Fig. 6e with Fig. 13 reveals that, following NaOL addition, under high shear conditions, particle aggregation predominantly occurs within the 20–50 μm range. This transformation involves particles in the −10 μm and 10–45 μm categories progressively coalescing into agglomerates spanning the 45–200 μm range. Notably, in contrast to the low shear condition, where an initial increase in the 10–45 μm fraction is followed by a subsequent reduction, the agglomerates formed under high shear conditions demonstrate immediate stability, with no reversal observed in the $N_{p'(10\text{-}45\ \mu m)}$ curve. This suggests that, at high shear rates, particle aggregation enters a stable phase rapidly, with the early aggregation phase being succinct and the system quickly attaining equilibrium.

The augmented collision frequency at elevated shear rates accelerates the formation of mid-sized aggregates, but the same forces inhibit further aggregation of smaller particles, thus restricting the growth of the agglomerates. Such dynamics underscore the rapid onset of flocculation under high shear, though with constrained agglomeration growth (Nogueira et al., 2023).

Fig. 14 corroborates these observations. Specifically, Fig. 14b reveals that, while some aggregation occurs post-NaOL addition, the aggregates formed are significantly smaller and more dispersed compared to those in Fig. 14a. This disparity can be attributed to the more intricate rheological interactions under turbulent conditions at high shear rates, where local shear forces, coupled with turbulence, impede the further enlargement of the aggregates (Neelakantan et al., 2018). These findings emphasize the dual role of high shear rates in the flocculation process—first enhancing particle aggregation efficiency during the early stages, but subsequently limiting further floc growth, as evidenced by the stabilization of particle size distributions.

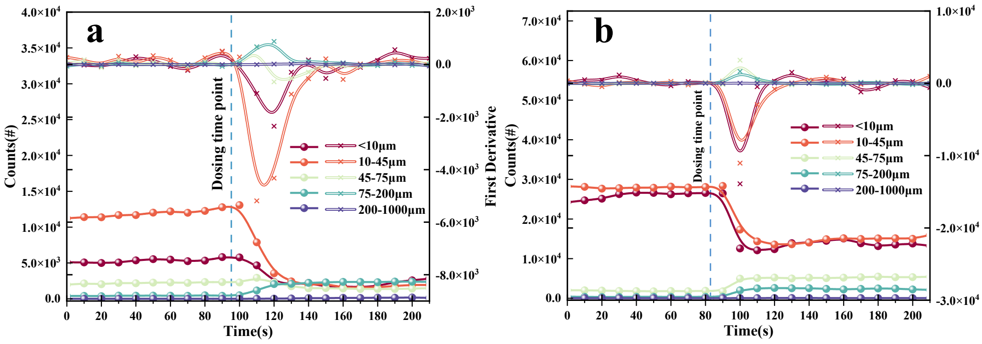

Fig. 13. Plot of particle size variation and first derivative: (a) Experiment 3 (Shear rate: 36.6 S^{-1}), (b) Experiment 12 (Shear rate: 73.4 S^{-1})

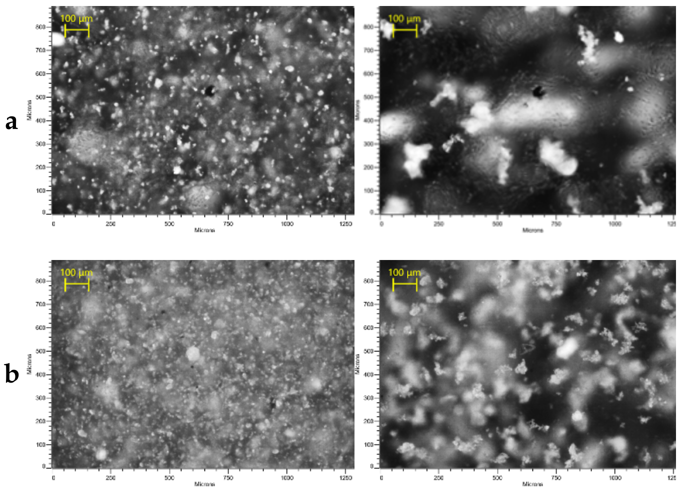

Before adding the collector Stabilization of flocs

Fig. 14. PVM captured image of floc variation over time: (a) Experiment 3 (Shear rate: 36.6 S^{-1}), (b) Experiment 12 (Shear rate: 73.4 S^{-1})

3.3. Flocculation kinetics discussion

To elucidate the effects of collector concentration, depressant concentration, pH, and shear rate on the flocculation dynamics of mixed mineral systems, the modified Smoluchowski model was utilized to interpret FBRM data. As a cornerstone of flocculation kinetics, the Smoluchowski model assumes that particle collisions in the liquid phase mediated by Brownian motion, shear forces, or turbulence, drive the formation of flocs (Negro et al., 2005). The particle aggregation rate was quantified using the flocculation index (k_{c1}), enabling the evaluation of floc formation and growth behavior as a function of particle concentration. These flocculation dynamics are mathematically represented by Eq. (5).

$$\frac{dn_c}{dt}=-k_{c1}n_c^2+k_{c2}n_c \tag{5}$$

In this model, n_c represents the particle count measured per second, t denotes the collector contact time (in seconds), and k_{c1} and k_{c2} are the flocculation and deflocculation indices, respectively. During the initial few seconds of flocculation, the deflocculation process can be neglected compared to flocculation. Furthermore, since the experiments were conducted under constant rotational speed, the effect of shear-induced deflocculation on the flocculation process can also be disregarded (Zhang et al., 2013). As a result, Eq. (5) can be simplified as follows:

$$n_c=\frac{n_{c0}}{n_{c0}k_{c1}t+1} \tag{6}$$

Here, n_{c0} represents the initial particle count in the system before the addition of the NaOL.

Błąd! Nie można odnaleźć źródła odwołania. Fig. 15 shows the variation in particle flocculation rates under different experimental conditions. Data points 22 and 15 correspond to low and high concentrations of the collector NaOL, respectively. Points 3, 24, 12, and 27 represent the low and high levels of depressant concentration and shear rate, while points 26 and 9 correspond to low and high pH values.

A comparison between Experiments 22 and 15 reveals that at lower NaOL concentrations, the flocculation index is notably reduced. Although flocculation still occurs, the rate is significantly slower, leading to a lower efficiency in floc formation. Similarly, Experiments 3 and 24, as well as Experiments 12 and 27, which correspond to low and high concentrations of the H_3PO_4 concentrations, show that the flocculation index is relatively insensitive to changes in H_3PO_4 concentration. The minor differences observed between the curves indicate that H_3PO_4 does not significantly influence the flocculation process. In contrast, the shear rate exerts a more substantial impact. At high shear rates (Experiments 12 and 27), the peak flocculation index is approximately 2.0×10^{-6} Counts^{-1} s^{-1} and declines rapidly. Conversely, at low shear rates (Experiments 3 and 24), the peak flocculation index is higher and the decline occurs more gradually, suggesting that lower shear rates promote more stable and efficient flocculation. When examining the effect of pH, a higher peak flocculation index is observed at elevated pH (Experiment 9), indicating a faster initial flocculation, though the process completes more quickly. In contrast, at lower pH (Experiment 26), the flocculation index remains more stable. While the initial rate is slower, the overall process follows a pattern of gradual increase, followed by a steady decline.

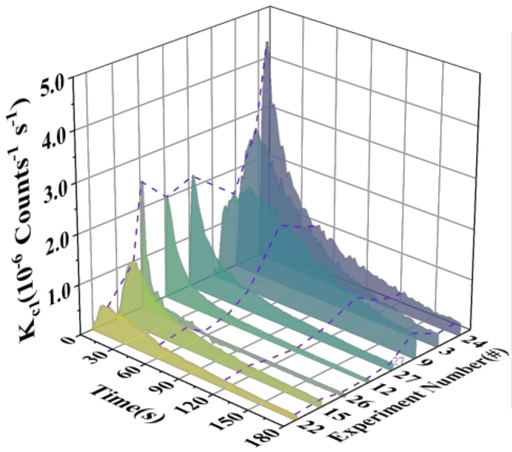

Std.	Collector Concentration (10^-4 mol/L)	Depressant Concentration (10^-4 mol/L)	pH	Shaer rate (S^-1)
22	1.0	1.0	7.0	55.0
15	10.0	1.0	7.0	55.0
26	5.5	50.5	11.0	36.6
12	5.5	1.0	7.0	73.4
27	5.5	100.0	7.0	73.4
9	5.5	50.5	3.0	36.6
3	5.5	1.0	7.0	36.6
24	5.5	100.0	7.0	36.6

Fig. 15. Variation in particle flocculation rates under different experimental conditions

Overall, the four factors exhibit significant differences in their effects on the various stages of the flocculation process, including the coalescence stage, the crushing stage, and the metastable stage. The coalescence stage is primarily influenced by factors such as particle surface charge and collision frequency (Wu et al., 2000; Zhe et al., 2021). Both NaOL concentration and shear rate jointly determine the upper limit of flocculation rate during this phase. A moderate increase in NaOL concentration and a reduction in shear rate can significantly enhance the initial flocculation rate, consistent with reported data (Wang et al., 2020). Conversely, the effects of H_3PO_4 concentration and pH on the initial phase are less pronounced. In the intermediate slow growth phase, most particles have already undergone initial collisions and aggregation, causing a noticeable slowdown in the flocculation rate (Niu et al., 2017). This stage is primarily controlled by pH, with markedly different trends observed under extreme pH conditions. Under acidic conditions, the slow growth period is extended, whereas under alkaline conditions, the system quickly reaches a stable phase. It is important to note that the mechanism of pH influence is complex; on one hand, pH affects the chemical properties of the reagents in the slurry, while on the other hand, it regulates the surface potential and reactivity of apatite and dolomite particles in the slurry (Ye et al., 2017). In the metastable stage, the system approaches equilibrium, and floc growth nearly ceases. At this stage, the main factors influencing floc stability and settling performance are NaOL concentration, pH, and shear rate, which collectively govern the outcome. This aligns with the observations of numerous researchers (Li et al., 2016; Li et al., 2021; Li et al., 2019). To clearly explain the impact of various factors on particle flocculation and flotation recovery, a multi-factor coupling mechanism model for the particle flocculation process was constructed, as shown in Fig. 16. As mentioned earlier, these four factors have different effects on particle flocculation, with the inhibitor having the least impact, while the other three factors exhibit dynamic regulatory characteristics at different stages of flocculation. Once the flocculated products enter the flotation system, their particle size distribution characteristics, in conjunction with the original control parameters, collaboratively determine the flotation potential of the particles. This synergistic effect is specifically reflected in: (1) the interfacial chemical environment established by the reagent system; (2) the coupling of mechanical shear forces and fluid viscosity in the turbulent flow field; and (3) the multi-scale distribution characteristics of the particle population. Notably, as a result of multi-parameter interactions, the particle size distribution not only carries the regulatory information from previous processing stages but also serves as a key mediating variable that directly influences the final flotation performance.

As previously mentioned, flocculation behavior not only directly affects the particle size distribution but also indirectly determines the bubble attachment efficiency and particle recovery rate during flotation. Therefore, the regulatory effects of the four factors on flocculation inevitably extend to changes in recovery. To analyze this relationship, a one-factor-at-a-time approach was applied in the response surface experiments, with the other three factors fixed at their zero-coded levels (Zhang, 2023). The effects of the four factors on both flocculation particle size and the flotation recovery rate are illustrated in Fig. 17, where the solid line represents particle size and the dashed line represents recovery rate. The coded values indicate the variation range of each factor from low (-1) to high (1) levels.

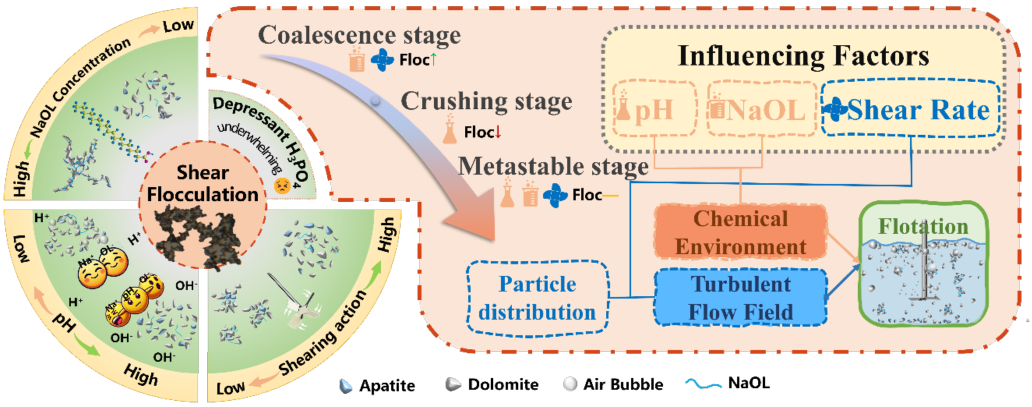

Fig. 16 Mechanism diagram of the effects of various factors on the shear flocculation stage

Fig. 17 provides further insight into the distinct effects of various factors on particle size and recovery. These factors exert significantly different influences on both particle size and recovery, with shear rate playing a particularly prominent role. An increase in shear rate disrupts the floc structure (Chen et al., 2022), resulting in smaller particle sizes and a subsequent decline in recovery. This reduction in recovery is attributed to two main factors: the weakened stability of particle-bubble attachment and the differential impact of shear-induced flow field changes on particles of different sizes. Higher shear rates intensify the turbulent energy in the flow, leading to a reduction in floc size (Liang et al., 2022), while also diminishing the capture efficiency of larger particles due to decreased interaction with the turbulent flow (Sun et al., 2022; Yan et al., 2022). The impact of pH on particle size and recovery demonstrates a nonlinear relationship. Under mildly alkaline conditions, particle size reaches its peak, and recovery is enhanced, suggesting that optimal pH levels facilitate both floc formation and an increase in particle hydrophobicity. In contrast, at extreme pH values, both particle size and recovery experience a significant decline, likely due to increased electrostatic repulsion between particles and the destabilization of the flocs.

In conclusion, the regulation of particle size distribution by these factors indirectly affects flotation performance. Floc size variations are crucial for flotation performance. The analysis shows that controlling particle size within an optimal range—through a combination of reagent dosage and shear flocculation—is essential for optimizing agglomeration flotation recovery.

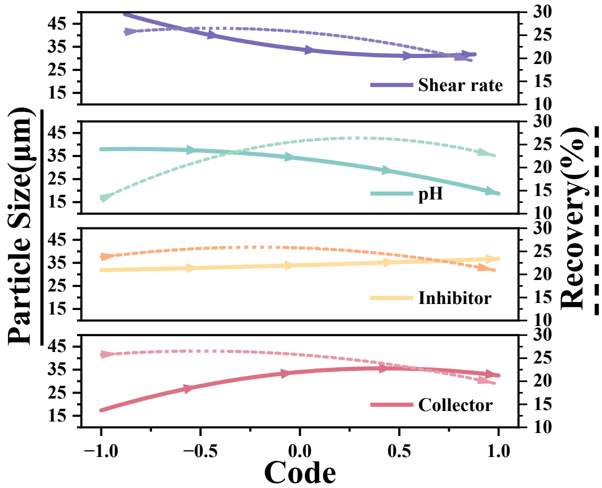

Fig. 17. Single-factor effect plot in response surface

4. Conclusions

A second-order regression model based on Box-Behnken experiments, combined with FBRM/PVM analysis, systematically characterized the flocculation dynamics of apatite-dolomite mixed ore. The key findings are:

1) The concentration of the collector NaOL, pH, and shear rate significantly influence the flocculation particle size of the mixed ore. pH exerted the strongest control on flocculation particle size (pH > NaOL concentration > shear rate). Regarding two-factor interactions, the interaction effect between pH and collector concentration is the most pronounced, with their synergistic effect playing a critical role in the flocculation process.
2) The results from FBRM and PVM indicate that NaOL concentration, pH, and shear rate affect flocculation behavior in distinct stages. During the coalescence stage, NaOL concentration and shear rate determine the upper limit of the flocculation rate. A moderate increase in NaOL concentration or a reduction in shear rate significantly accelerates the flocculation process. In the crushing stage, the flocculation rate slows down, with pH becoming the dominant factor. In the metastable stage, the system approaches equilibrium, and floc stability and sedimentation performance are influenced by a combination of NaOL concentration, pH, and shear rate. The synergistic effect of these three factors ultimately governs the final state of the floc.
3) Shear rate affects floc structure and flotation performance by altering the intensity of the flow field, while pH plays a pivotal role in modulating the surface chemistry of particles and their size distribution. Optimal conditions improve size uniformity and recovery, whereas extremes trigger floc destabilization and efficiency loss. Process optimization thus requires synergistic balance between turbulence and chemical environments for optimal performance.

Acknowledgments

The research was funded by the National Natural Science Foundation of China (52164018). Additionally, we extend our gratitude to the Analytical Testing Center of Shanghai Jiao Tong University for their invaluable assistance with the experiments.

References:

BOXALL, J. A., KOH, C. A., SLOAN, E. D., SUM, A. K., WU, D. T., 2010. *Measurement and calibration of droplet size distributions in water-in-oil emulsions by particle video microscope and a focused beam reflectance method*. Ind. Eng. Chem. Res. 49, 1412-1418.

CAI, Z., LUO, H., WU, J., LIU, X., 2019. *Shearing flocculation flotation of low-grade collophanite in jinning*. Multipurpose Util. Miner. Res. 49-54.

CHEN, W., ZHANG, G., ZHU, Y., 2022. *Rheological investigations of the improved fine scheelite flotation spiked with agitation medium*. Int. J. Min. Sci. Technol. 32, 1379-1388.

CHIMONYO, W., PENG, Y., 2022. *Selective inhibition of kaolinite entrainment during chalcopyrite flotation in saline water*. Miner. Eng. 184, 107637.

DUAN, J., 2022, Cfd-pbm coupling simulation of coal escence crushing efficiency in flocculation process of fine coal slime, Taiyuan University of Technology, Taiyuan, China.

GAO, R., ZHOU, K., ZHANG, J., GUO, H., REN, Q., 2019. *Research on the dynamic characteristics in the flocculation process of mineral processing tailings*. Ieee Access. 7, 129244-129259.

GRABSCH, A. F., YAHYAEI, M., FAWELL, P. D., 2020. *Number-sensitive particle size measurements for monitoring flocculation responses to different grinding conditions*. Miner. Eng. 145.

GREGORY, J., 2013. *Flocculation fundamentals: encyclopedia of colloid and interface science*, Springer Berlin Heidelberg, Berlin, Heidelberg.

HAO, C., GUO, J., CHU, M., YANG, Y., WANG, L., GONG, Y., ZHAO, X., 2019. *Analysis of models and factors of long flame coal flotation process by response surface methodology*. J. Min. Sci. Technol. 4, 547-557.

HE, G., ZHANG, Q., 2023. *Study on mechanism of selective inhibition of fluorapatite and dolomite by amino trimethylene phosphonic acid*. Industrial Minerals & Processing. 52, 12-17.

HUANG, X., ZHANG, Q., 2023. *Interaction behavior between coarse and fine particles in the reverse flotation of fluorapatite and dolomite*. Langmuir. 39, 12931-12943.

HUANG, X., ZHANG, Q., 2024. *Depression mechanism of acid for flotation separation of fluorapatite and dolomite using tof-sims and xps*. J. Mol. Liq. 394, 123584.

JIN, S., 2022, Study on hydrophobic aggregation flotation of fine cassiterite using hydroxamic acids as collectors, Central South University, Hunan, China.

LASENTEC, M., 2001. *Product group. Fbrm® d600 hardware manual. Mettler-toledo autochem*. Inc., Redmond, Wa.

LI, D., YIN, W., LIU, Q., CAO, S., SUN, Q., ZHAO, C., YAO, J., 2017. *Interactions between fine and coarse hematite particles in aqueous suspension and their implications for flotation*. Miner. Eng. 114, 74-81.

LI, D., YIN, W., SUN, C., YAO, J., 2020. *Aggregation characteristics of fine hematite and siderite particles in aqueous suspension*. Powder Technol. 368, 286-296.

LI, D., ZHONG, H., YIN, W., SUN, C., HU, Y., 2021. *Particle aggregation characteristics of hematite-quartz mixture with addition of sodium oleate*. Powder Technol. 393, 796-806.

LI, L. I., SAI, Z., QIANG, H. E., XUE-BIN, H. U., 2015. *Application of response surface methodology in experiment design and optimization*. Res. Explor. Lab. 34, 41-45.

LI, M., XIANG, Y., CHEN, T., GAO, X., LIU, Q., 2021. *Separation of ultra-fine hematite and quartz particles using asynchronous flocculation flotation*. Miner. Eng. 164, 106817.

LI, S., GAO, L., CAO, Y., GUI, X., LI, Z., 2016. *Effect of ph on the flocculation behaviors of kaolin using a ph-sensitive copolymer*. Water Sci. Technol. 74, 729-737.

LI, S., GAO, L., WANG, J., ZHOU, H., LIAO, Y., XING, Y., GUI, X., CAO, Y., 2021. *Polyethylene oxide assisted separation of molybdenite from quartz by flotation*. Miner. Eng. 162, 106765.

LI, Y., XIA, W., WEN, B., XIE, G., 2019. *Filtration and dewatering of the mixture of quartz and kaolinite in different proportions*. J. Colloid. Interface. Sci. 555, 731-739.

LIANG, L., TIAN, F., WANG, M., 2022. *Enhancement of selective flocculation of quartz in coal flotation based on shear rate adjustment*. J. China Univ. Min. Technol. 51, 988-997.

LUO, H., ZHAO, Z., CAI, Z., ZHANG, Z., YAN, Y., GUO, Y., 2021. *Recovery of medium to low grade phosphate rock stockpiled in jinning phosphate mine by shear flocculation flotation*. Industrial Minerals & Processing. 50, 26-30.

NEELAKANTAN, R., VAEZI G., F., SANDERS, R. S., 2018. *Effect of shear on the yield stress and aggregate structure of flocculant-dosed, concentrated kaolinite suspensions*. Miner. Eng. 123, 95-103.

NEGRO, C, FUENTE, E, BLANCO, A, TIJERO, J, 2005. *Flocculation mechanism induced by phenolic resin/peo and floc properties*. Aiche J. 51, 1022-1031.

NIU, F., CHEN, Y., ZHANG, J., LIU, F., WANG, Z., 2024. *Selective flocculation-flotation of ultrafine hematite from clay minerals under asynchronous flocculation regulation*. Int. J. Min. Sci. Technol. 34, 1563-1574.

NIU, F., LI, Z., ZHANG, J., 2017. *Study on flocculation kinetics of fine hematite in stirring flow field*. Conserv. Util. Miner. Resour. 58-63.

NOGUEIRA, F., RODRIGUES, K., PEREIRA, C., SILVA, A. C., SILVA, E. M. S., AZIZI, A., HASSANZADEH, A., 2023. *Quartz fine particle processing: hydrophobic aggregation by shear flocculation*. Minerals. 13, 1208.

PASCOE, R. D., DOHERTY, E., 1997. *Shear flocculation and flotation of hematite using sodium oleate*. Int. J. Miner. Process. 51, 269-282.

RUAN, Y., HE, D., CHI, R., 2019. *Review on beneficiation techniques and reagents used for phosphate ores*. Minerals. 9, 253.

RUAN, Y., ZHANG, Z., LUO, H., XIAO, C., ZHOU, F., CHI, R., 2018. *Effects of metal ions on the flotation of apatite, dolomite and quartz*. Minerals. 8, 141.

SHI, J., 2017, Research on behaviors and mechanism of dispersion of the fine collophane and dolomite, Guizhou University, Guiyang, in China.

SUN, C., SHI, S., HAN, D., 2022. *Zoning model of flotation kinetics process in air-forced mechanical agitator flotation machine*. J. China Univ. Min. Technol. 51, 411-418.

WANG, C., SUN, C., LIU, Q., 2020. *Formation, breakage, and re-growth of quartz flocs generated by non-ionic high molecular weight polyacrylamide*. Miner. Eng. 157, 106546.

WANG, H., DU, H., WANG, J., ZHANG, F., CAO, S., 2024. *Unconfined compressive strength of composite improved expansive soil based on response surface method*. Sci. Technol. Eng. 24, 6854-6861.

WANG, X., 2020, Surface wettability regulation of minerals in flotation of calcium-magnesium phosphate ore, Guizhou University, Guiyang, in China.

WANG, X., ZHOU, S., BU, X., NI, C., XIE, G., PENG, Y., 2021. *Investigation on interaction behavior between coarse and fine particles in the coal flotation using focused beam reflectance measurement (fbrm) and particle video microscope (pvm)*. Sep. Sci. Technol. 56, 1418-1430.

WANG, Z., WU, A., RUAN, Z., BURGER, R., WANG, S., MO, Y., 2024. *Flocculation behavior, mechanics, and optimization of tailings based on multi-objective: insight into the concentration and time-dependent floc size*. Powder Technol. 439.

WEI, H., GAO, B., REN, J., LI, A., YANG, H., 2018. *Coagulation/flocculation in dewatering of sludge: a review*. Water Res. 143, 608-631.

WU, D., TAN, F., WANG, X., XIU, C., ZHANG, H., 2000. *Study of kinetics mechanism of flocculation and controlling index*. Environ. Eng. 22-25.

WU, Y., ZHANG, Y., LI, X., GUAN, Z., HE, Q., 2024. *Advancements in studying the flocculation flotation of fine minerals*. Conserv. Util. Miner. Res. 44, 16-26.

XIE, J., 2024. *Selective removal of dolomite from rare earth element-bearing phosphorite by flotation and leaching and the adsorption mechanism of agents on mineral surfaces*. Surf. Interface Anal. 56, 82-98.

YAN, X., WANG, W., ZHANG, H., LI, D., SUN, Z., YANG, H., 2022. *Enhancement of liquid-solid mixing and particle hydrophobization by an impeller-less flotation pulp conditioning device*. Miner. Eng. 190, 107933.

YANG, B., HUANG, P., SONG, S., LUO, H., ZHANG, Y., 2018. *Hydrophobic agglomeration of apatite fines induced by sodium oleate in aqueous solutions*. Results Phys. 9, 970-977.

YANG, J., 2020, Formation mechanism of hydrophobic agglomerates of fine-grained scheelite and its application in alkali leaching slag of scheelite, Beijing University of Science and Technology, Beijing, China.

YANG, P., HU, X., ZI, F., YANG, B., WANG, Q., CHEN, Y., CHEN, S., 2020. *Synergistic enhancement of fine-kaolinite-particle hydrophobic agglomeration by combining dodecylamine with octanoic acid*. Miner. Eng. 155, 106444.

YE, J., 2019, Study on interfacial regulation of fine apatite flotation, Guizhou University, Guiyang, in China.

YE, J., WANG, X., LL, X., CHL, X., ZHANG, Q., 2017. *Effects of acid on adsorption of collector on collophane and dolomite surface*. J. Wuhan Inst. Technol. 39, 565-570.

YE, J., ZHANG, Q., LL, X., WANG, X., SHEN, Z., MAO, S., 2020. *In-situ investigation of hydrophobic agglomeration of fine dolomite*. Min. Metall. Eng. 40, 39-42.

ZHANG, F., LI, G., PEI, J., WANG, C., WANG, H., WANG, Q., 2013. *Study on the dynamic flocculation process of kaolin suspensions induced by cationic polyacrylamide by using fbrm*. China Pulp & Paper. 32, 15-20.

ZHANG, G., YAN, D., YANG-GE, Z., QI-MING, F., WEI-QING, W., 2011. *Influence of ph on adsorption of sodium oleate on surface of ilmenite and titanaugite*. J. Cent. South Univ. 42, 2898-2904.

ZHANG, L., CHEN, Y., ZHAO, B., 2024. *Numerical simulation of the optimization for the inlet structure of the furnace in the phosphogypsum reduction process by sulfur vapor*. Powder Technol. 438.

ZHANG, Q., LI, X., MAO, S., ZHANG, T., 2023. *Application progress of molecular simulation in phosphate ore flotation*. J. Min. Sci. Technol. 8, 102-114.

ZHANG, Q., MAO, S., HUANG, X., CHEN, A., ZHANG, W., 2024. *Research progress in surface chemistry of flotation for apatite and gangue minerals in phosphate ore*. Conserv. Util. Miner. Res. 44, 1-15.

ZHANG, Y., 2023, Study on flocculation and sedimentation characteristics of two types of iron tailings in liaoning region, Liaoning Technical University, Liaoning, China.

ZHAO, L., CHEN, A., ZHANG, Q., GAO, G., 2022. *Study on mineral hydrophobic agglomeration behavior and slurry rheology in microfine apatite-dolomite flotation system*. Conserv. Util. Miner. Res. 42, 104-111.

ZHAO, L., ZHANG, Q., 2024. *Study of oleic acid-induced hydrophobic agglomeration of apatite fines through rheology*. Miner. Eng. 218, 108911.

ZHE, L., WENGANG, Z., 2021. *Flocculation process of coal slime water based on flocculation kinetics and its research methods: a critical review*. China Min. Mag. 30, 160-167.